Chain Dynamics, Conformations, and Phase Transformations for Form III Polymorph of Isotactic Poly(1-butene) Investigated by High-Resolution Solid-State ^{13}C NMR Spectroscopy and Molecular Mechanics Calculations

Toshikazu Miyoshi,*,† Shigenobu Hayashi,‡ Fumio Imashiro,§ and Akira Kaito†

Research Center of Macromolecular Technology, National Institute of Advanced Industrial Science and Technology (AIST), Central 5, 1-1-1 Higashi, Tsukuba, Ibaraki 305-8565, Japan, Institute for Materials & Chemical Process, National Institute of Advanced Industrial Science and Technology (AIST), Central 5, 1-1-1 Higashi, Tsukuba, Ibaraki 305-8565, Japan, and Department of Chemistry, Graduate School of Science, Kyoto University, Kyoto 606-8502, Japan

Received November 12, 2001

ABSTRACT: High-resolution solid-state ^{13}C NMR spectroscopy and MM3 molecular mechanics calculations have been applied to investigate side-chain conformations, side- and main-chain dynamics, and phase transformations of the form III polymorph of *isotactic*-poly(1-butene) (*i*-PB). MM3 calculations indicate that the $t-g'$ side-chain conformation is much more stable than the $g'-g$ and $g-t$ side-chain conformations in the crystal lattices of form III. The ^{13}C cross-polarization magic-angle spinning (CPMAS) NMR spectrum at 199 K shows that the methyl group in the side chain adopts only the $t-g'$ conformation. Upfield shift for the ^{13}C methyl signal above 338 K indicates dynamic disorder in the side-chain conformations. The ^{13}C two-dimensional exchange NMR reveals that the polymer chains in form III consist of two components. The 74% polymer chains execute the 90° helical jump motion with an activation energy of 79.3 ± 5.6 kJ/mol, while the residual chains are immobile. It is found that the 90° helical jump motion begins to occur at the temperature very close to the glass-transition temperature (T_g). Upfield shifts for the ^{13}C main-chain signals at 338 K indicate the motional mode change from the 90° helical jump motion to "more or less" rotational or jump motion with different angle displacements. Above 338 K, two phase transformations from form III to forms II and I′ are confirmed in the ^{13}C CPMAS spectra. The ^{1}H spin−lattice relaxation times in the rotating frame show that the transformation from form III to form I′ proceeds within the form III phase via the crystal-to-crystal process, whereas the line-shape analyses of the ^{13}C direct-polarization magic-angle spinning (DPMAS) NMR spectra indicate that the transformation from form III to form II proceeds via the quasi-melting/recrystallization process. The frozen chain conformations in the amorphous phase below T_g are also investigated on the basis of the ^{13}C chemical shifts. It is suggested that most of the main chains adopt the helical $(tg')_n$ conformation, and the residual part adopts the (tt) conformation.

Introduction

Chain dynamics plays important roles in the bulk properties of polymers, which has been characterized in both the crystalline and amorphous phases by dynamic-mechanical, dielectric-relaxation measurements,[1] and solid-state NMR spectroscopy.[2] In the past decade, two-dimensional (2D) exchange NMR spectroscopy[3] has been developed and applied to elucidate exact motional modes and correlation times of the chain dynamics in both the phases of polymers.

The main-chain conformations are distributed in the amorphous phase, and conformational transition[4] and continuous rotational motion[5] occur above glass transition temperature (T_g). Their correlation times around T_g were shown to obey the Williams−Landel−Ferry (WLF)[6] equation. On the other hand, the polymer chain adopts a well-defined conformation in the crystalline phase. For examples, polyethylene (PE) adopts the all-trans conformation $(tt)_n$, and *isotactic*-poly(propylene) (*i*-PP) and polyoxymethylene (POM) adopt 3_1 and 9_5 helical conformations $(tg')_n$, respectively, though their dihedral angles are different between them. These polymers show large-amplitude motions around their chain axes between the neighboring sites, accompanying translation.[3,7−10] PE,[8] *i*-PP,[9] and POM[10] perform 180° chain flip motion and 120° and 200° helical jump motions, respectively. There is a common character describing the large-amplitude motions in the crystalline polymers: The jump rates obey the Arrhenius-type temperature dependence, and their motions continue up to melting temperatures (T_m) without changing their motional modes. Previous investigations have been limited to the polymers without side chains[8,10] or with only a methyl group[9] as the side chain. Therefore, it is interesting to extend a detailed dynamics investigation to a crystalline polymer with flexible and long side chains.

Isotactic-poly(1-butene) (*i*-PB) is a crystalline polymer and has an ethyl group as the side group. X-ray diffraction studies showed that *i*-PB has four polymorphs depending on the formation conditions: form I, twinned hexagonal with a 3_1 helix;[11] form I′, untwined hexagonal with a 3_1 helix;[12] form II, tetragonal with an 11_3 helix;[13] and form III, orthorhombic with a 4_1 helix.[14] All of the helical main chains for I(I′)−III adopt the common $(tg')_n$ conformation, though their dihedral angles are slightly different.[15,16] There are three possible

† Macromolecular Technology Research Center, AIST.
‡ Institute for Materials & Chemical Process, AIST.
§ Kyoto University.
* To whom corresponding author should be addressed. E-mail t-miyoshi@aist.go.jp; Tel 81-298-61-6283; Fax 81-298-61-6243.

10.1021/ma011961g CCC: $22.00
Published on Web 03/03/2002

conformations for the side chain under the $(tg')_n$ main-chain conformation, which are expressed as the $t-g'$, $g'-g$, and $g-t$ conformations (vide infra) with the combined use of the two dihedral angles around the side-chain methylene carbon−methine carbon bond, where signs of the dihedral angles for g and g' are different from each other. It was assumed in the X-ray diffraction analysis that the methyl conformation in the side chain adopts only the $t-g'$ conformation.

High-resolution solid-state ^{13}C NMR spectroscopy is also a powerful tool to investigate polymer conformations. Belfiore et al.[17] showed that the ^{13}C chemical shifts of the main-chain signals of *i*-PB depend on the dihedral angles in the main chain of each form. Maring et al.[18] investigated the side-chain conformation in form I in the wide temperature range. They insisted that the side-chain conformation in form I adopts the $t-g'$, $g-t$, and $g'-g$ conformations below $T_g = 248-253$ K[19] and that a rapid exchange among them occurs above T_g. In their investigation, however, the contribution of the amorphous signals to the spectra was ignored even below T_g. This may affect their conclusions on the side-chain conformation. Some other solid-state NMR methods were also applied to elucidate the chain dynamics in various forms of *i*-PB.[18−20] Maring et al. suggested using the ^1H broad-line and relaxation measurements[19] that the polymer chains in forms I and I′ are rigid well above T_g, while those in forms II and III are mobile. ^{13}C 2D exchange NMR spectroscopy was applied to the investigation of the molecular motions in *i*-PB. Maring et al.[18] demonstrated that the polymer chain in form III undergoes the 90° helical jump motion at 273 K. However, the motional behaviors in form III of *i*-PB at temperatures around T_g and T_m (363−373 K)[21−24] have not well been understood. Therefore, it is not clear whether the side-chain conformation and dynamics correlate with the main-chain dynamics of *i*-PB in form III or not.

Besides NMR spectroscopy, various methods such as X-ray diffraction,[21,22] differential scanning calorimetry (DSC),[22,23] differential thermal analysis (DTA),[21,24] dilatometry,[21] and IR[24] showed that form III undergoes two phase transformations into forms I′ and II near T_m, though relations between the phase transformations and the molecular motions in form III were not well elucidated. Moreover, the transformation mechanisms are unclear up to now.

In this article we describe the side-chain conformation and dynamics and the main-chain dynamics for form III of *i*-PB in the wide temperature range of 199−381 K as well as the conformations in the amorphous phase. We have measured variable temperature ^{13}C high-resolution cross-polarization (CP) and direct-polarization (DP) magic-angle spinning (MAS) NMR spectra and ^{13}C spin−lattice relaxation times in the laboratory frame (T_1) and have performed MM3 molecular mechanics calculations[25] to investigate the side-chain conformation and its dynamics in form III and the conformations in the amorphous phase. We have also measured variable temperature ^{13}C 2D exchange NMR spectra to elucidate the dynamic behavior of the 90° helical jump motion around T_g. ^{13}C CPMAS NMR spectra are also used for investigating the chain dynamics in form III at temperatures just below those of the phase transformations and melting. ^1H spin−lattice relaxation times in the rotating frame ($T_{1\rho}$) lead us to clarify the mechanism of the phase transformation from form III to form I′. Through these investigations, we will demonstrate characteristic chain dynamics of *i*-PB as a crystalline polymer with a side chain.

Experimental Section

Sample Preparation. The polymer sample of *i*-PB with a weight-averaged molecular weight (M_w) of 185 000 was purchased from Poly Science Co. Ltd. The virgin sample with the isotacticity of more than 90% consisted of the form I and the amorphous phases. It was dissolved into toluene at concentrations of 0.5% (wt %). The solution was heated at 363 K for 10 min and kept at room temperature for 3 days. The precipitate appearing gradually was collected and dried at room temperature for 1 day and then at 323 K under a reduced pressure for 1 day, yielding the form III-rich sample. We could not obtain the T_g value for the form III-rich sample by DSC measurements with heating rates of 5−20 K/min. In the present work, we use the minimum value ($T_g = 248$ K) for *i*-PB in the literature.[18−20]

The mixed sample of forms III and I′, heat-treated form III, was prepared by heating the form III-rich sample in an oil bath at 368 K for 1 h. The amorphous sample was obtained by quenching the virgin sample into a liquid nitrogen bath after keeping it in an oil bath at 413 K (above T_m of form I) for 5 min. Special attention was paid for the amorphous sample, because the amorphous chains immediately crystallize into form II even at room temperature due to its low T_g. The NMR probe was cooled and maintained at 240 K before the measurements, and the NMR rotor containing the amorphous sample was immediately introduced into the probe from a liquid nitrogen bath while keeping the probe temperature below T_g.

NMR Measurements. The NMR experiment was carried out on a Bruker ASX200 NMR spectrometer with transmitter frequencies of 200.1 MHz for ^1H and 50.3 MHz for ^{13}C. The high-resolution solid-state ^{13}C NMR spectra were obtained by the combined use of high-power ^1H dipolar decoupling (DD) and MAS. ^{13}C chemical shifts were expressed with respect to tetramethylsilane by using the carbonyl carbon of glycine (176.48 ppm) as an external reference. The amplitudes of the radio-frequency pulses were set at about 57 kHz for both ^1H and ^{13}C. The MAS frequency was set at 2.0 kHz. The CP method was used with a contact time of 1.0 ms. The repetition time was varied from 4.0 to 8.0 s. Temperatures in the NMR probe were calibrated using methanol[26] and ethylene glycol.[27] The experimental errors for the temperatures were within ±1 K.

The DP method was also used with a repetition time of 8.0 s to determine the crystalline/amorphous ratio in each sample. This delay time was long enough for the magnetization of the methyl carbon to relax fully to the thermal equilibrium. The ^{13}C 2D exchange NMR spectra were taken using the time proportional phase increment method. The sampling points were 512 and 180−256 along t_2 and t_1, respectively. The dwell time between the sampling points was 200 μs in both time domains. ^1H $T_{1\rho}$ was measured using a ^1H spin-lock sequence followed by CP (the contact time of 300 μs) and detection through ^{13}C resonances. ^{13}C T_1 was measured using Torchia's method.[28]

Molecular Mechanics Calculations. The model lattice of form III of *i*-PB was assembled with seven pentamers of 1-butene, where the coordinates of the carbon atoms were fixed to those reported for form III of *i*-PB by X-ray crystallography,[14] and those of the hydrogen atoms were optimized by MM3 molecular mechanics calculations. The dihedral driver option was applied to obtain stable side-chain conformations and barriers to rotation of the side chain and the methyl group.

Results

^{13}C CPMAS and DPMAS NMR Spectra. Figure 1 shows the ^{13}C CPMAS NMR spectra of the form III-rich sample of *i*-PB below room temperature. The four signals observed at 14.6, 28.7, 36.8, and 41.3 ppm at

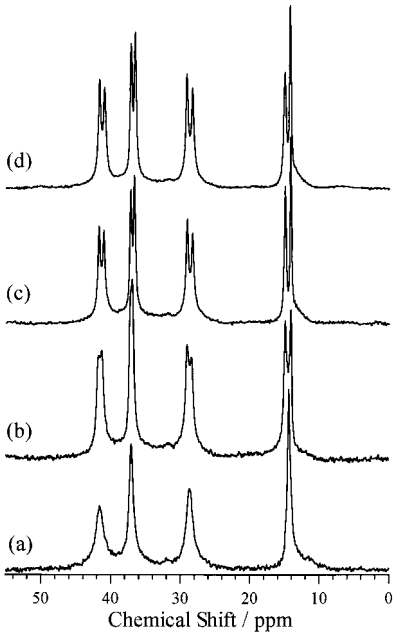

Figure 1. ^{13}C CPMAS NMR spectra of the form III-rich sample of *i*-PB at (a) 296, (b) 272, (c) 251, and (d) 199 K.

Table 1. ^{13}C Chemical Shift Values (ppm) of *i*-PB in Various Phases

	temp (K)	m-methylene	methine	s-methylene	methyl
form I′	367	38.6	31.5	26.9	12.6
		38.0		26.2	
form II	370	39.9	34.2	27.7	11.8
form III	296	41.3	36.8	28.7	14.6
	338	37.8	32.5	27.2	13.0
amorphous	199	38.8	33.9	28.4	13.3
				19.8	7.3

296 K (Figure 1a) are assigned to the methyl, side-chain methylene (s-methylene), methine, and main-chain methylene (m-methylene) carbons, respectively, and they are listed in Table 1. With lowering temperature, all the signals begin to split into doublet peaks with equal intensities at 272 K (Figure 1b). With further decreasing temperature, the line widths for the main-chain and s-methylene signals decrease and reach constant values of 25 and 23 Hz, 18 and 17 Hz, and 24 and 24 Hz for the high- and low-field sides of the s-methylene, methine, and m-methylene signals, respectively, at 251 K (Figure 1c), whereas the line width for the methyl signal broadens at temperatures below 251 K. At 199 K (Figure 1d), the line width (23 Hz) of the methyl signal at 15.1 ppm is broader than that (14 Hz) at 14.3 ppm. The observed doublet signals are attributed to the existence of noncongruent two sites, sites A and B, for the constitutional repeating units in form III as illustrated in Figure 2.[14,18] The merge of the split signals above 272 K results from the rapid dynamical exchange between sites A and B within the polymer chains. This exchange is brought about by the 90° helical jump motion of the polymer chains around their helical axes in the crystal lattice.[18]

Parts a and b of Figure 3 show the ^{13}C CPMAS NMR spectra for the amorphous and form III-rich samples, respectively, at 199 K. The broad signals around 7.3 and 13.3 ppm, 19.8 and 28.4 ppm, 33.9 ppm, and 38.8 ppm in the amorphous sample at 199 K are assigned to methyl, s-methylene, methine, and m-methylene carbons, respectively (Table 1). The spectrum of the form

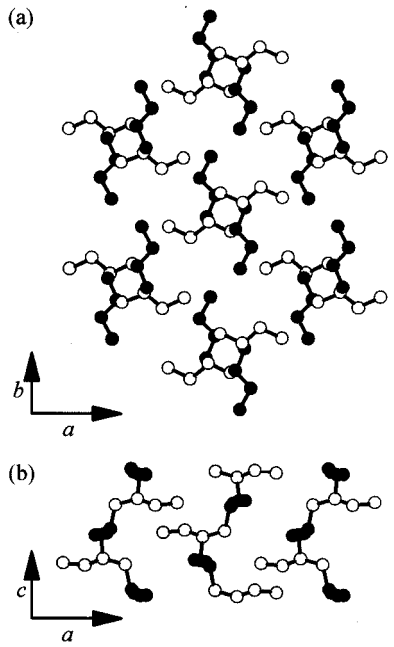

Figure 2. Form III model lattice consisting of seven pentamers of 1-butene. Only carbon atoms are drawn with circles, and their coordinates are those reported for form III of *i*-PB by X-ray crystallography.[14] The open and filled circles denote noncongruent sites A and B, respectively. (a) Projection on the *ab* plane. (b) Projection on the *ac* plane.

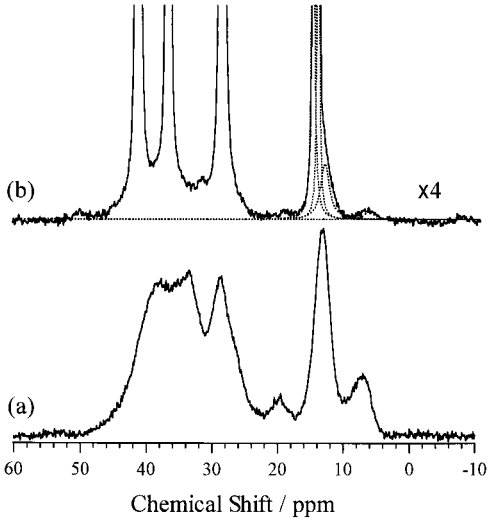

Figure 3. ^{13}C CPMAS NMR spectra at 199 K for (a) the amorphous phase and (b) the form III-rich sample. The latter spectrum is cut at a level of 25% of the highest peak. The dotted lines in the latter spectrum show the best-fitted ones for the observed spectrum in the methyl region.

III-rich sample also shows broad signals at the bottom of the doublet signals originated from form III. Their line shapes are similar to those of the amorphous sample, suggesting that the broad signals can be attributed to the amorphous phase in the form III-rich sample. Assuming that the structure of the present amorphous sample is the same as that of the amorphous phase in the form III-rich sample, we perform the line-shape fitting of the methyl signals with four Lorentzian functions, as shown in Figure 3b. The intensity ratio for the form III phase to the amorphous one is 81/19. The application of the same procedure to the DPMAS NMR spectrum yields the same intensity ratio. Thus,

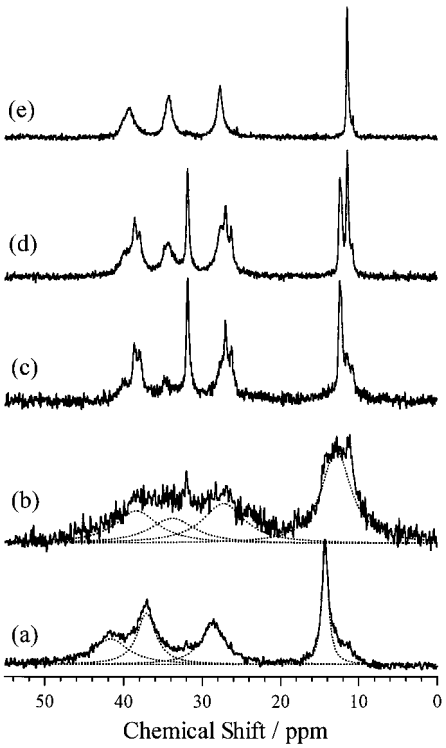

Figure 4. ^{13}C CPMAS NMR spectra for the form III-rich sample at (a) 316, (b) 338, (c) 367, (d) 370, and (e) 381 K. The dotted lines in (a) and (b) show the form III signals fitted to the spectra.

the crystallinity of the form III-rich sample used in this study is concluded to be 81%.

Figure 4 shows the ^{13}C CPMAS NMR spectra for the form III-rich sample at and above 316 K. Belfiore et al.[17] showed previously that the chemical shifts of the main-chain and s-methylene signals depend on the helical conformations. We can thus get information about the phase transformations from form III into forms I′ and II through the resolved ^{13}C signals. The form III signals mainly dominate the observed spectra up to 338 K (Figure 4a,b). The dotted lines show the signals of form III. The line widths of all the signals in form III become broader at 316 K (Figure 4a) compared to those at 296 K. This broadening originates from the motional broadening due to the interference between molecular motion and ^{1}H DD.[29,30] The chemical shift values for all the signals do not move up to 316 K. At 338 K, the line widths become much broader in all the signals, and all the signals move upfield. The chemical shifts are listed in Table 1.

The signals of forms I′ and II are also observed above 338 K. Their chemical shifts are almost independent of temperature. Table 1 lists the signal assignments and chemical shifts of form I′ at 367 K and II at 370 K. At 338 K, the methine signal of form I′ appears at 31.5 ppm with a small intensity. At 367 K, the form III signals almost disappear, the signals corresponding to forms I′ are clearly observed, and the form II signals also appear with a small intensity, as shown in Figure 4c. Further increasing temperature leads to an enhancement of the form II signals and disappearance of the form I′ signals (Figure 4e). Only the form II signals are detected in the CPMAS NMR spectrum at 381 K. It is noted that the amorphous signals are hardly observed above 316 K, because of inefficiency of CP for the amorphous phase at temperatures well above T_g.

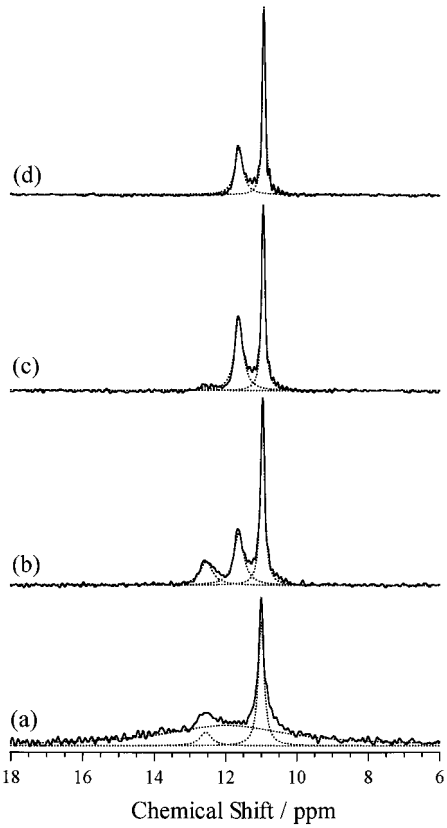

Figure 5. ^{13}C DPMAS NMR spectra for the methyl region of the form III-rich sample at (a) 361, (b) 370, (c) 377, and (d) 381 K. The dotted lines mean the best-fitted ones for the observed spectra. The methyl signals at 11.0, 11.8, and 12.6 ppm are assigned to the amorphous phase, form II, and form I′, respectively. The broad signal at 12.0 ppm at 361 K is attributed to form III.

Table 2. Component Ratios (%) for Forms I′, II, and III, and the Amorphous Phase at Various Temperatures on the Basis of the Peak Deconvolution for the Methyl Signals in the ^{13}C DPMAS NMR Spectra

temp (K)	form I′	form II	form III	amorphous
199			81.0	19.0
361	4.4		73.2	22.4
367	8.3		57.3	34.5
370	19.7	33.0		47.3
373	8.3	44.0		47.6
377	3.5	47.0		49.5
381		40.7		59.3

The transformations from form III into forms I′ and II can also be detected in the methyl region. The ^{13}C DPMAS NMR spectra of the form III-rich sample are taken at various temperatures in order to estimate the component ratios of the individual phases. Figure 5 shows the methyl region of the spectra. The most striking feature is a significant contribution from the amorphous phase (11.0 ppm) in the temperature range studied. The line-shape fitting for the observed spectrum is performed with a Lorentzian function for each signal, and the results are listed in Table 2. The content of form III decreases from 73.2% at 361 K to 57.3% at 367 K and then suddenly becomes 0.0% at 370 K. The amount of the amorphous phase increases monotonically with increasing temperature above 361 K. The content of form I′ also increases with increasing temperature from 361 K, reaches a maximum value of 19.7% at 370 K, and disappears completely at 381 K. The amount of form II increases suddenly to 33.0% at 370 K and increases

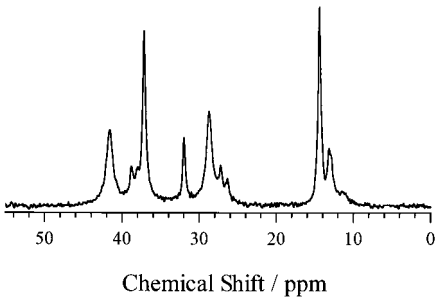

Figure 6. ^{13}C CPMAS NMR spectra of heat-treated form III of *i*-PB measured at 296 K. Form III was heat-treated at 368 K for 1 h.

up to 47.0% at 377 K. Further increasing temperature induces melting of form II. Although small signals originated from forms I′ and II are observed in the CPMAS spectrum at 338 and 367 K, respectively (Figure 4b,c), they are not detected in the DPMAS spectrum due to the low content less than ca. 2%.

^{1}H $T_{1\rho}$ Measurements. Figure 6 shows the ^{13}C CPMAS NMR spectra of heat-treated form III measured at 296 K after the heat treatment at 368 K for 1 h. The heat treatment above 338 K induces a partial transformation from form III into form I′. The phase structures of forms I′ and III after the partial transformation are investigated by using the ^{1}H dipole−dipole interaction, since the dipole−dipole interaction is inversely proportional to the third power of the internuclear distance.[31] There are some techniques for measuring spin diffusion between the different phases.[32] Among them, measurement of the ^{1}H spin−lattice relaxation time is a convenient and simple way to examine the phase structure in the heterogeneous system. The ^{1}H spin−lattice relaxation times in the laboratory frame (^{1}H T_1) and in the rotating frame (^{1}H $T_{1\rho}$) allow us to evaluate the domain size of the heterogeneous system on scales of 200−400 and 20−40 Å, respectively, if the component polymers have different relaxation times.[32] We measure ^{1}H $T_{1\rho}$ at room temperature for the form III-rich sample before and after the heat treatment. All the signals in each form show similar ^{1}H $T_{1\rho}$ values within the experimental errors. We use the ^{1}H $T_{1\rho}$ values obtained through the methine carbons. The ^{1}H $T_{1\rho}$ value for form III is 6.9 ± 0.5 ms before the heat treatment. The value for form III increases to 16.0 ± 0.8 ms after the heat treatment, which is essentially consistent with that (17.7 ± 1.4 ms) for form I′.

There are two possible mechanisms for the change of the ^{1}H $T_{1\rho}$ values of form III before and after the heat treatment. One is motional change of form III. The other is spin diffusion between the form I′ and form III phases. The ^{13}C line width is also sensitive to molecular motions with a frequency of ^{1}H DD field strength. After the heat treatment, the form III signals show the motional broadening above 316 K (data are not shown) as observed for the form III-rich sample before the treatment (Figure 4b), whereas the line widths of the form I′ signals in heat-treated form III are almost constant up to melting (data are not shown). These results show that the form I polymer chains are rigid in the heat-treated form III sample, whereas the form III polymer chains are mobile after the heat treatment as well as before the treatment. This is supported by the previous investigation.[19] The ^{13}C line-width data, thus, indicate that the spin diffusion between the forms I′ and III phases leads to the similar ^{1}H $T_{1\rho}$ values. Namely, form I′ does not form domains, the size of which is larger than ca. 40 Å, but mixes homogeneously with the form III crystalline phase.

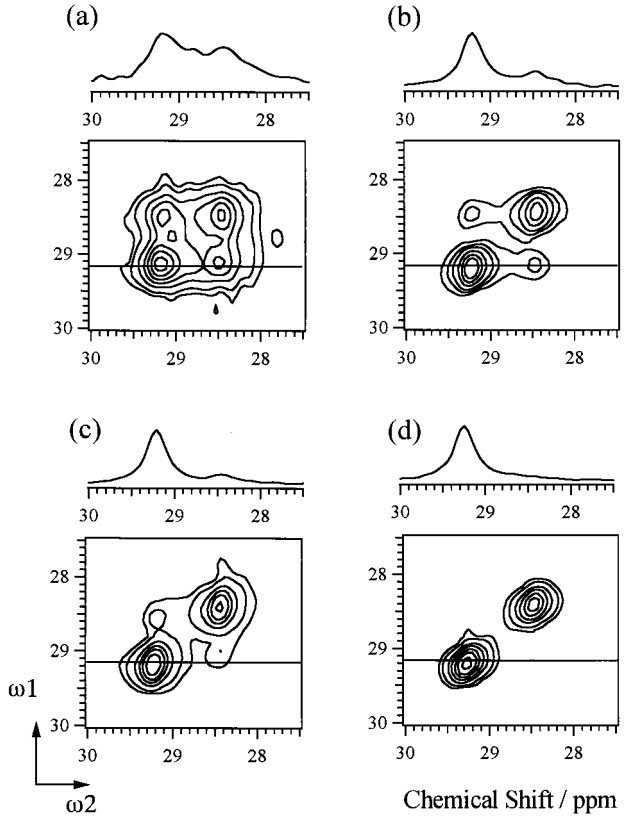

Figure 7. ^{13}C 2D exchange NMR spectra for the s-methylene region of form III at (a) 272, (b) 251, (c) 240, and (d) and 219 K. The mixing time (τ_m) is set at 1 s. The six contour levels are drawn with exponential spacings between 10 and 80% of the maximum spectral height. The cross sections at solid lines are also shown.

2D Exchange NMR Spectra. The application of the 2D exchange NMR to the 90° helical jump motion in form III has been discussed.[18] In the present work, we have measured the 2D exchange NMR spectra at various temperatures, especially around T_g. Figure 7 shows the spectra for the s-methylene region with a mixing time (τ_m) of 1 s. Although the cross-peak intensities reduce with decreasing temperature, they are still observed at 240 K, below the reported T_g value (248 K) (Figure 7c), and disappear completely at 219 K (Figure 7d). They are not detected even when increasing τ_m up to 2 s at this temperature (the spectrum is not shown), indicating that the ^{13}C−^{13}C spin-diffusion effect can be ignored. The cross-peak intensity, therefore, leads us to the quantitative analysis for the 90° helical jump motion. Figure 8a plots the cross/diagonal peak intensity ratios ($I_{cross}/I_{diagonal}$) obtained at various values of τ_m and temperatures. At 272 K, $I_{cross}/I_{diagonal}$ reaches a value of ca. 0.74 at τ_m = 300 ms, and it is almost constant up to τ_m of 2 s. The dependence of $I_{cross}/I_{diagonal}$ on τ_m is expressed[33] as

$$I_{cross}/I_{diagonal} = p[1 + \exp(-2k\tau_m)]/[1 - \exp(-2k\tau_m)] \quad (1)$$

where p is the population of the chain segments performing the 90° helical jump motion and k is the jump rate. Parameters are evaluated by fitting the

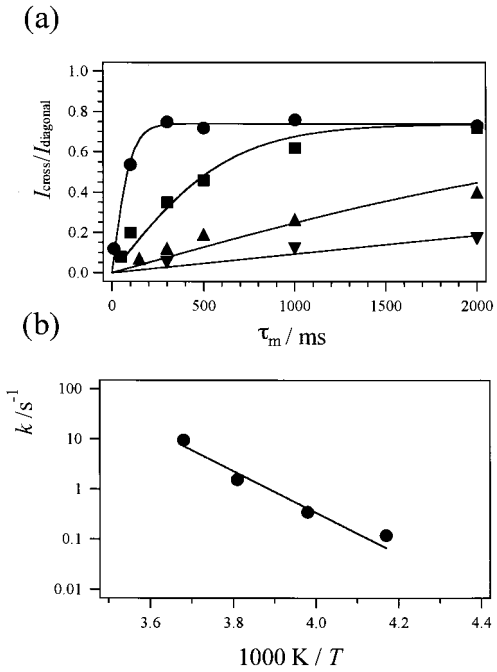

Figure 8. (a) Mixing time (τ_m) dependence of the cross/diagonal peak intensity ratios ($I_{cross}/I_{daiagonal}$) for the s-methylene signals of form III at (●) 272, (■) 261, (▲) 251, and (▼) 240 K. The solid lines show the best-fitted ones for the experimental data with eqs 1. (b) Temperature dependence of the jump rate for the 90° helical jump motion in form III. The solid line is the best-fitted one to the experimental data.

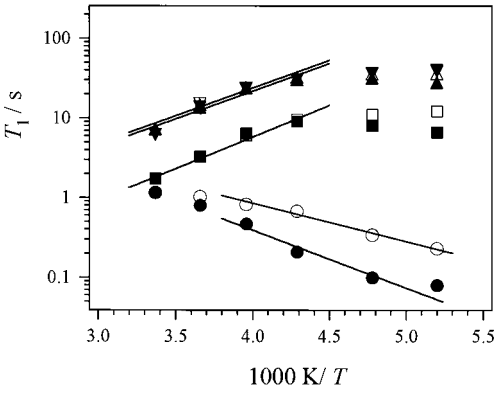

Figure 9. Temperature dependence of the ^{13}C T_1 values. Circles, squares, triangles, and upside-down triangles stand for the T_1 values of the methyl, s-methylene, methine, and m-methylene carbons, respectively. The open and filled symbols relate to the high- and low-field signals, respectively. The solid lines show the best-fitted curves to the experimental data with eqs 2 or 3.

experimental data at 272 K to eq 1, which are $p = 0.74 \pm 0.03$ and $k = 9.6 \pm 0.8$ s^{-1} at this temperature. This indicates that 74% of the chain segments are mobile at 272 K, while the other segments are essentially immobile. The experimental data below 261 K are analyzed with eq 1 on the assumption that p is 0.74. The best-fitted lines are drawn with solid ones in Figure 8a, and the obtained exchange rates are plotted in Figure 8b. This plot shows that the temperature dependence of the exchange rate is represented with a single-exponential function around T_g. The jump rates can well be represented in terms of the Arrhenius function with the activation energy, E_a, of 79.3 ± 5.8 kJ/mol.

^{13}C T_1 Measurements. The ^{13}C spin−lattice relaxation time in the laboratory frame (^{13}C T_1) is very useful

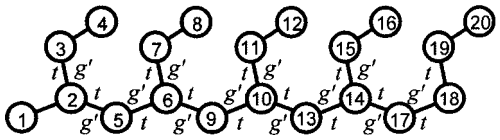

Figure 10. Numbering of the carbon atoms and all of the conformations around C−C bonds for the pentamers of 1-butene in the model lattice drawn in Figure 2. The main and side chains adopts the $(tg')_n$ and $t-g'$ conformations, respectively.

to investigate local motions of the functional groups. The relaxation curves of all the signals in form III are described by single-exponential functions in the temperature range 193−296 K. The obtained ^{13}C T_1 values are plotted in Figure 9. The ^{13}C T_1 values for the methyl carbon decrease with decreasing temperature, suggesting that the ^{13}C T_1 minima should appear below 193 K. The T_1 values for the s-methylene carbons increase with decreasing temperature, become bent around 233 K, and then decrease gently. The differences between the ^{13}C T_1 values for the sites A and B are apparent below 253 K for the methyl carbons and below 233 K for the s-methylene carbons. The temperature dependence of the ^{13}C T_1 values for the main-chain carbons are roughly consistent with that for the s-methylene carbons, though the splitting between the ^{13}C T_1 values for the two sites are not observed in the present temperature range.

Assuming that the ^{13}C−^{1}H dipole−dipole interactions are responsible for ^{13}C T_1, the high- and low-temperature sides of the ^{13}C T_1 curves are written with eqs 2 and 3, respectively

$$1/T_1 \propto \tau_0 \exp(E_a/RT) \quad (2)$$

$$1/T_1 \propto \tau_0 \exp(-E_a/RT) \quad (3)$$

where E_a is the activation energy for the molecular motion and R is the gas constant. We analyze the ^{13}C T_1 values below 253 K for the methyl carbons and those above 233 K for the s-methylene and main-chain carbons. The E_a values are 13.0 ± 2.4 and 9.2 ± 0.9 kJ/mol for the ^{13}C methyl signals at 15.1 and 14.3 ppm, respectively, indicating the existence of the motional heterogeneity between the two sites in the form III polymer chains. The values for the m-methylene and methine carbons above 233 K are 13.7 ± 0.7 and 13.4 ± 0.7 kJ/mol, respectively, which are much smaller than that for the 90° helical jump motion (79.3 kJ/mol), and are close to that for the s-methylene carbons above 233 K (15.2 ± 1.5 kJ/mol). These results suggest that the s-methylene motion is responsible for ^{13}C T_1 of the main-chain carbons above 233 K.

Molecular Mechanics Calculations. Figure 10 indicates the numbering of the carbon atoms and all of the C−C−C−C dihedral angles for the pentamer of 1-butene in the model lattice (Figure 2) in the $(tg')_n$ main-chain and the $t-g'$ side-chain conformations. It should be noted that a single crystal of form III contains either right- or left-handed helical chains.[14] In this work, we consider mainly the right-handed one, which corresponds to the $(tg')_n$ main-chain conformation. The rotational potentials are calculated with the dihedral drive option in MM3 calculations. The driven dihedral angles for the side-chain and methyl group rotations are the C9−C10−C11−C12 and C10−C11−C12−H dihedral angles, respectively, of the central pentamer in the model lattice. Fixed coordinates are used for all the carbon atoms in the surrounding six pentamers and for

the main-chain carbon atoms in the central one during the calculations. It is noted that the C9−C12 atoms in the model lattice shown in Figure 2 belong to site A. The rotational potentials for site B are calculated using the model lattice shifted by one constitutional repeating unit along the *c* axis.

The calculated steric energies of the model lattices (SE_L) for the $g'-g$ side-chain conformation in sites A and B are higher by 30.4 and 14.8 kJ/mol, respectively, than those for the $t-g'$ side-chain conformation in the corresponding model lattices. The barriers to the conformational transition from the $t-g'$ conformation to the $g'-g$ one are 40.1 and 51.5 kJ/mol for sites A and B, respectively. The SE_L for the $g-t$ side-chain conformation in site A is higher by 54.1 kJ/mol than that for the $t-g'$ side-chain conformation, whereas the side chain in site B has no stable structure in the $g-t$ conformation. The $g-t$ side-chain conformation has negligible contribution in the side-chain conformations. The barriers to rotation of the methyl groups in the $t-g'$ conformation are calculated to be 13.9 and 9.8 kJ/mol for sites A and B, respectively.

Discussion

Side-Chain Conformations in Form III. MM3 calculations for the model lattice of form III indicate that the $t-g'$ and $g'-g$ conformations are available for the side chain, though the former is much more stable than the latter. The $g'-g$ side-chain conformation yields an upfield shift of ca. 5 ppm for the ^{13}C methyl signal compared to the $t-g'$ side-chain conformation due to the so-called γ-gauche effect[34] on the ^{13}C chemical shifts. The observed small splitting of the ^{13}C methyl signals (15.1 and 14.3 ppm at 199 K) in form III is attributed not to the γ-gauche effect but to the small difference between the geometries in sites A and B. The side-chain conformation in form III at 199 K is concluded to be $t-g'$ in accord with the assumption in the X-ray study.[14] The upfield shifts of the ^{13}C methyl signals above 338 K is ascribed to the increase in the population of the $g'-g$ side-chain conformation with a rapid transition between the $t-g'$ and $g'-g$ side-chain conformations. Therefore, it is concluded that the side chain in form III is dynamically disordered above 338 K.

Chain Conformations in the Amorphous Phase. Here, we try to obtain conformational information in the amorphous phase on the basis of the ^{13}C chemical shifts, though chain conformations in the amorphous phase are more complicated than those in the crystalline phase. It is noted that the signal of the s-methylene carbon allows us to view the detailed main-chain conformation in the amorphous phase, because its position is affected by rotation around the next nearest C−C bonds. Thus, the ^{13}C chemical shift of the s-methylene carbon reflects directly the main-chain conformation. Only three conformations illustrated schematically in Figure 11 are allowed for *i*-PB roughly when successive gg' conformations can be omitted in various combinations of conformations due to steric repulsion.

Two signals are observed at 28.4 and 19.8 ppm for the s-methylene carbons (Figure 3a). The broad main signal at 28.4 ppm covers the chemical shift range for the s-methylene carbons in the various forms I′, II, and III (Figure 4), indicating that most of the main chains in the amorphous phase adopt the $(tg')_n$ conformation with slightly distributed dihedral angles. The second signal at 19.8 ppm is not found in forms I(I′)−III and should be attributed to the specific conformation of the main chain in the amorphous phase. The s-methylene carbon in form I′ adopts the typical $(tg')_n$ conformation which shows the signals at 26.2 and 26.9 ppm (Figure 4). Thus, an additional shielding of 6.4−7.1 ppm for the second s-methylene signal requires an additional γ-gauche effect. Thus, the second signal at 19.8 ppm is responsible for the (*tt*) main-chain conformation as shown in Figure 11c, which should be possible to exist in the amorphous phase.

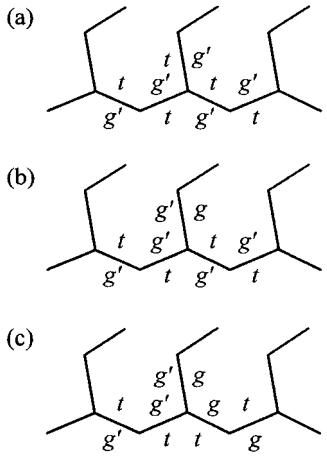

Figure 11. Three allowed conformations for *i*-PB. The main chains in (a) and (b) adopt the ...$g'(tg')t$... conformation, and that in (c) adopts the ...$g'(tt)g$... conformation. The side chain in (a) adopts the $t-g'$ conformation, and those in (b) and (c) adopt the $g'-g$ conformation.

The ^{13}C methyl signals apparently show two separated signals at 13.3 and 7.3 ppm at 199 K. The former can be attributed to the $t-g'$ conformation in Figure 11a and the latter to the $g'-g$ conformations in Figure 11b,c. The sharp ^{13}C methyl signal at 11.0 ppm above 361 K in the amorphous phase (Figure 5) shows the existence of a rapid conformational transition between the two conformations.

Packing Effects on the Side-Chain Mobility in Form III. The 90° helical jump motion becomes slow below 272 K compared to the chemical shift differences between the doublet signals. We can thus investigate the side-chain mobility of the two sites in form III through the resolved signals. The ^{13}C T_1 measurements (Figure 9) and the line widths at 199 K (Figure 1e) for the ^{13}C methyl signals clearly show that the methyl group mobilities are different between sites A and B in form III. The obtained experimental E_a values of 13.0 and 9.2 kJ/mol for the methyl carbons at 15.1 and 14.3 ppm, respectively, are consistent with the calculated barriers of 13.9 and 9.8 kJ/mol for the methyl groups in sites A and B, respectively. The resonance signals at 15.1 and 14.3 ppm can therefore be assigned to the methyl carbons in sites A and B, respectively.

The calculated energy barriers (40.1 and 51.5 kJ/mol for A and B sites, respectively) for the conformational transition between the $t-g'$ and $g'-g$ conformations indicate mobility differences between them. The transition is caused by the s-methylene motion. The T_1 values of the s-methylene carbons in the two sites do not show apparent differences above 233 K. The T_1 values in the two sites are averaged out by the 90° helical jump motion, since the spin−lattice relaxation rates for s-methylene carbons (0.3 s^{-1} at 272 K) are much smaller than the helical jump rate (9.6 s^{-1} at 272 K). The

obtained E_a (15.2 kJ/mol) from the ^{13}C T_1 values of the s-methylene carbon is much smaller than the calculated values responsible for the conformational transition between the $t-g'$ and $g'-g$ ones. Such a difference suggests that the conformational transition is not reflected in the ^{13}C T_1 values and that different types of motions dominate the ^{13}C T_1 values.

Main-Chain Dynamics in Form III. It is found that the 74% polymer chain in form III executes the 90° helical jump motion with the jump rate of 9.6 s^{-1} at 272 K, while the rest is immobile. Such a dynamic heterogeneity suggests that the form III crystalline structure is heterogeneous. The jump rates decrease with decreasing temperature. The 90° helical jump motion is still active at 240 K just below the reported T_g value (248 K). In our investigation, we could not obtain the exact T_g value for the amorphous phase in the form III-rich sample. Hence, we conclude that the 90° helical jump motion begin to occur at the temperature very close to T_g.

The observed low starting temperature for the 90° helical jump motion in form III is attributed to a low density of form III of *i*-PB (0.897 g/cm^3).[14] This is supported by the previous investigations on the densities and the chain dynamics[20] for *i*-PB in the various forms. Forms I and I′ show higher density (0.950 g/cm^3)[35] than those of forms II (0.920 g/cm^3)[36] and III. Maring et al.[19] showed using ^1H broad line and relaxations time measurements that the polymer chains in forms I and I′ do not show the main-chain dynamics at temperatures close to their T_m's, whereas those in forms II and III are mobile above T_g.

The 90° helical jump motion in form III is accelerated with increasing temperature, and this motion leads to motional broadenings of the ^{13}C signals at 316 K. Upfield shifts are observed for the ^{13}C signals of all the carbons at 338 K (Table 1). The upfield shift for the methyl carbon is attributed to increase in the population of the $g'-g$ side-chain conformation accompanied by the rapid conformational transition or the dynamical conformational disorder, as discussed above. The m-methylene carbon has two methyl and two methine carbons at its γ positions. Thus, the increase in the population of the $g'-g$ side-chain conformation contributes also to the upfield shifts for the ^{13}C m-methylene signal. The observed upfield shift for the m-methylene signal (3.5 ppm) is, however, much larger than that for the methyl one (1.6 ppm) (Table 1). Furthermore, the chemical shift of the methine carbon is affected by only the main-chain conformations on the basis of the γ-gauche effect. Therefore, the observed upfield shifts of the main-chain carbons indicate that the conformational change of the main chain of form III occurs above 338 K. This means that the pure 90° helical motion does not persist and changes to a "more or less" rotational or jump motion with different angle displacements.

The polymer chains show "more or less" rotational motions in the crystalline phases of poly(acrylonitrile) (PAN)[37] and form II of 1,4-*trans*-poly(butadiene) (*t*-PBD).[38] Kaji et al.[39−41] investigated recently the exact conformations for PAN, using $^{13}C-^{13}C$ double quantum[39, 40] and $^2H-^{13}C$ heteronuclear multiple-quantum correlation NMR spectroscopy,[41] and concluded that the main chain shows static conformational disorder due to steric hindrance and electric dipole interaction. De Rosa et al.[42] suggested using packing energy calculation that static conformational disorder exists in form II of *t*-PBD. It is, thus, indicated that "more or less" rotational motions in these two polymers are attributed to the static conformational disorders. The polymer chain in form III of *i*-PB, however, adopts a well-defined conformation (4_1 helix) in the static state as well as those in the other semicrystalline polymers such as PE,[8,43] POM,[10] and *i*-PP.[9,44] Among them, the polymer chain only in form III of *i*-PB shows the motional mode change with increasing temperature. As shown above, *i*-PB has an ethyl group as the side chain which is possible to affect the conformational energy map of the main chain. In fact, dynamic disorder of the side chain in form III of *i*-PB is observed at temperatures above 338 K where motional change of the 90° helical jump motion occurs. It is reasonably concluded from these facts that the side-chain mobility is an origin of the motional and conformational changes in form III of *i*-PB.

Phase Transformations of Form III. Two mechanisms should be considered when one crystalline phase undergoes a transition to the other: One is the crystal-to-crystal process, and the other is the quasi-melting/recrystallization process. The former and the latter take place inside and outside of the form III phase, respectively. The previous DTA[21] and DSC[23] measurements observed an endothermic peak corresponding to melting of form III and a following exothermic peak which shows the crystallization of the amorphous phase to form II. Previous X-ray diffraction and dilatometry studies[21] could, however, give no evidence for the appearance of the amorphous phase after melting of form III.

Our present experiments clearly show that the form II phase immediately grows after melting of the form III phase, whereas the amorphous signals continuously increase above 361 K (Table 2). These observations indicate that the transformation from form III into form II proceeds via the quasi-melting/recrystallization process. This situation is slightly different in the transformation from form III to form I′. The form I′ signals are clearly visible at 361 K before complete melting of the form III phase at 370 K. Moreover, the ^1H $T_{1\rho}$ experiments elucidate that the form I′ phase mixes intimately with the form III phase on the scale shorter than ca. 40 Å. This denies the transformation from form III to form I′ via the quasi-melting/recrystallization process. If the transformation occurred outside the form III phase due to the quasi-melting, the polymer chains in the form III phase would not interact directly with those in the form I′ phase, and each phase would be surrounded by the amorphous phase. Such a phase structure should have led to inconsistency of the ^1H $T_{1\rho}$ values for the forms III and I′ phases.

On the contrary, the polymer chains in form I′ interact directly with those in form III if the transformation proceeds via the crystal-to-crystal process. Such a phase structure should lead to the common ^1H $T_{1\rho}$ values for both phases as observed. It is, thus, indicated that the transformation from form III to form I′ proceeds via the crystal-to-crystal process.

The crystal-to-crystal process from form III into form I′ directly requires the conformational change from a 4_1 helix to a 3_1 one within the form III phase. The polymer chains in form III perform the 90° helical jump motion with a 4_1 helical conformation above 240 K, as discussed already. The polymer chains in form III change their motional mode also, when they perform the conformational change under the transformation. These were confirmed by the ^{13}C chemical shift change

of the form III signals above 338 K. On the other hand, the quasi-melting/recrystallization process is not related to the chain dynamics in form III, because form II appears after melting of form III. Therefore, the above specific chain dynamics of form III around T_m might be the origin of the two independent transformations in the similar temperature regions.

Summary

In this study, the characteristic chain dynamics and conformations of the form III polymorph of *i*-PB were investigated in the wide temperature range, employing 1D and 2D ^{13}C NMR spectroscopy. The results are summarized as follows.

(1) The methyl group in form III adopts only the $t-g'$ conformation at 199 K. The population of the $g'-g$ conformation increases above 338 K, and a rapid transition between the $t-g'$ and $g'-g$ conformations becomes apparent. Namely, the side chain is dynamically disordered above 338 K.

(2) The 90° helical jump motion in form III begins to occur at the temperature very close to T_g. The jump rates are found to obey Arrhenius type dependence. This high mobility is explained in terms of the low density of form III. The 90° helical jump motion cannot persist and changes to rotational or jump motion with different angle displacements above 338 K, where the side chain shows an apparent transition between the $t-g'$ and $g'-g$ conformations. It is, thus, indicated that the side-chain mobility affects the main-chain dynamics of *i*-PB.

(3) There are two different processes for the transformations from form III into forms I′ and II near T_m. The former proceeds within the form III phase via the crystal-to-crystal process, and the latter takes place outside of the form III phase via the quasi-melting/recrystallization one.

Through these investigations, it is demonstrated that the side-chain conformations and mobility play important roles in the overall chain dynamics and the phase transformations in form III of *i*-PB.

References and Notes

(1) Boyd, H. R. *Polymer* **1985**, *26*, 323−347.
(2) Komorowski, R. A. *High-Resolution NMR Spectroscopy of Synthetic Polymers in Bulk*; VCH Publishers: New York, 1986.
(3) Schmidt-Rohr, K.; Spiess, W. H *Multidimensional Solid-State NMR and Polymers*; Academic Press: London, 1994.
(4) Zemke, K.; Chmelka, F. B.; Schmidt-Rohr, K.; Spiess, W. H. *Macromolecules* **1991**, *24*, 6874−6876.
(5) Kaufmann, S.; Weifing, D.; Schaefer, D.; Spiess, W. H. *J. Chem. Phys.* **1990**, *93*, 197−214.
(6) Williams, M. L.; Landel, R. F.; Ferry, J. D. *J. Am. Chem. Soc.* **1955**, *77*, 3701.
(7) Hu, G.-W.; Schmidt-Rohr, K. *Acta Polym.* **1999**, *50*, 271−285.
(8) Hu, G.-W.; Boeffel, C.; Schmidt-Rohr, K. *Macromolecules* **1999**, *32*, 1611−1619.
(9) Kentgens, A. P. M.; de Boer, E.; Veeman, W. S. *J. Chem. Phys.* **1987**, *87*, 6859−6865.
(10) Hagemeyer, A.; Schmidt-Rohr, K.; Spiess, W. H. *Adv. Magn. Reson.* **1989**, *13*, 85−130.
(11) Miller, R.; Holland, V. F. *Polym. Lett.* **1964**, *2*, 519−521.
(12) Natta, G.; Corradini, P.; Bassi, I. W. *Nuovo Cimento Suppl.* **1960**, *15*, 52−67.
(13) Petraccone, V.; Pirozzi, B.; Corrasini, P. *Eur. Polym. J.* **1976**, *12*, 323−327.
(14) Cojazzi, G.; Malta, V.; Celotti, G.; Zannetti, R. *Macromol. Chem.* **1976**, *177*, 915−926.
(15) Ajo, D.; Granozzi, G.; Zanneti, R. *Makromol. Chem.* **1977**, *178*, 2471−2481.
(16) Corradini, P.; Napolitano, R.; Peterccone, V. *Eur. Polym. J.* **1984**, *20*, 931−934.
(17) Belfiore, L. A.; Schilling, F. C.; Tonelli, A. E.; Lovinnger, A. J.; Bovey, F. A. *Macromolecules* **1984**, *17*, 2561−2565.
(18) Maring, D.; Whilhelm, M.; Spiess, W. H.; Meurer, B.; Weill, G. *J. Polym. Sci., Part B: Polym. Phys.* **2000**, *38*, 2611−2624.
(19) Maring, D.; Meurer, B.; Weill, G. *J. Polym. Sci., Part B: Polym. Phys.* **1995**, *33*, 1235−1247.
(20) Beckham, W. H.; Schmidt-Rohr, K.; Spiess, W. H. *ACS Symp. Ser.* **1995**, 242−253.
(21) Geacintov, C.; Schotlan, S. R.; Miles, B. R. *J. Polym. Sci., Part C* **1964**, *6*, 197−207.
(22) Nakamura, K.; Aoike, T.; Usaka, K.; Kanamoto, T. *Macromolecules* **1999**, *32*, 4975−4982.
(23) Gohil, M. P.; Patel, D. R. *Macromol. Chem.* **1977**, *64*, 43−57.
(24) Goldbach, G.; Peitscher, G. *Polym. Lett.* **1968**, *6*, 783−788.
(25) Allinger, N. L.; Yuh, Y. H.; Lii, J. H. *J. Am. Chem. Soc.* **1989**, *111*, 8551−8566.
(26) VanGeet, L. A. *Anal. Chem.* **1970**, *42*, 679−680.
(27) Raiford, S. D.; Fisk, L. C.; Becker, D. E. *Anal. Chem.* **1970**, *51*, 2050−2051.
(28) Torchia, D. A. *J. Magn. Reson.* **1978**, *30*, 613−616.
(29) Vanderhart, D. L.; Earl, W. P.; Garroway, A. N. *J. Magn. Reson.* **1981**, *44*, 361−401.
(30) Rothwell, W. P.; Waugh, J. S. *J. Chem. Phys.* **1981**, *74*, 2721−2732.
(31) Abragam, A. *The Principles of Nuclear Magnetism*; Oxford University Press: London, 1961.
(32) Takegoshi, K. *Annu. Rep. NMR Spectrosc.* **1995**, *30*, 97−126.
(33) Ernst. R. R.; Bodenhausen, G.; Wokaun, A. *Principles of Nuclear Magnetic Resonance in One and Two Dimensions*; Clarendon: Oxford, 1987.
(34) Zemke, K.; Schmidt-Rohr, K.; Spiess, W. H. *Acta Polym.* **1994**, *45*, 148−159.
(35) Wunderlich, B. *Macromolecular Physics*; Academic Press: New York, 1973; Vol. 1.
(36) Tadokoro, H. *Structure of Crystalline Polymers*; Wiley-Interscience: New York, 1979.
(37) Thomsen, T.; Zachmann, G. H.; Korte, S. *Macromolecules* **1992**, *25*, 6934−6937.
(38) Möller, M. *Makromol. Chem., Rapid Commun.* **1988**, *9*, 107−114.
(39) Kaji, H.; Schmidt-Rohr, K. *Macromoleclules* **2000**, *33*, 5169−5180.
(40) Kaji, H.; Schmidt-Rohr, K. *Macromolecules* **2001**, *34*, 7368−7381.
(41) Kaji, H.; Schmidt-Rohr, K. *Macromolecules* **2001**, *34*, 7382−7391.
(42) De Rosa, C.; Napolitano, R.; Pirozzi, B. *Polymer* **1986**, *26*, 2039−2042.
(43) Schmidt-Rohr, K.; Spiess, W. H. *Macromolecules* **1991**, *24*, 5288−5293.
(44) Saito, S.; Moteki, Y.; Nakagawa, M.; Horii, F.; Kitamaru, R. *Macromolecules* **1990**, *23*, 3256−3260.

MA011961G